

Supporting Information

Beyond the Universal Volume Scaling: Tailoring Two-Photon Absorption in Nanomaterials by Heterostructure Design

Arthur Alo,¹ Leonardo W.T. Barros,¹ Gabriel Nagamine,¹ Jonathan C. Lemus,¹ Josep Planelles,² José L. Movilla,³ Juan I. Climente,² Hak June Lee,^{4,5} Wan Ki Bae,⁵ and Lazaro A. Padilha ^{1}*

¹*Instituto de Física “Gleb Wataghin”, Universidade Estadual de Campinas, UNICAMP, P.O. Box 6165, 13083-859 Campinas, Sao Paulo, Brazil*

²*Dept. de Química Física i Analítica, Universitat Jaume I, 12080, Castelló, Spain;*

³*Dept. d'Educació i Didàctiques Específiques, Universitat Jaume I, 12080, Castelló, Spain;*

⁴*School of Chemical and Biological Engineering, Seoul National University, Seoul 08826, Republic of Korea;*

⁵*SKKU Advanced Institute of Nanotechnology (SAINT), Sungkyunkwan University (SKKU), Suwon 16419, Republic of Korea*

e-mail: padilha@ifi.unicamp.br

Additional Two-Photon Absorption Cross-Section Data Analysis

To understand further the influence of the CdS shell on the two-photon absorption of CdSe/CdS heterostructures, we have analyzed the data from the CdSe/CdS with 2.0 nm core series considering only the samples with thin (thick) shells. The analysis indicates that the volume dependence becomes stronger for larger shells. This could be explained by the increased influence from the shell, as it is discussed in details in the main text.

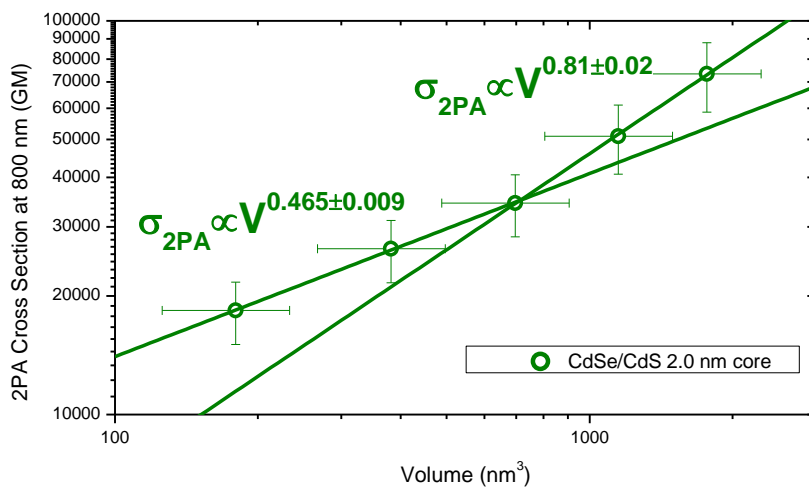


Figure S1. Two-photon absorption cross-section data for the CdSe/CdS samples with 2.0 nm core fitted in two different groups, the first 3 points and the last 3 points. The fittings suggest a higher volume dependence of the two-photon absorption cross-section for samples with thicker shells.

Theoretical Modeling Methods

Electron and hole states are calculated using single-band effective mass Hamiltonians as in Ref. ¹. For simplicity, we assume constant mass all over the structure. For electrons, we choose $m_e=0.20m_0$, and for heavy holes $m_h=0.60m_0$, with m_0 the mass of a free electron. These values closely correspond to those of CdSe -notice however that the electron mass is greater than that of bulk CdSe, $m_e=0.13m_0$. This is to account for band non-parabolicity, which is relevant to the dimensions we study. ² A bulk band gap of 1.75 eV is taken for CdSe, ³ Conduction band offsets are 0.3 eV (CdSe/CdS) ⁴ and 0.72 eV

(CdSe/ZnCdS).⁵ Subsequently, valence band offsets are 0.44 eV (CdSe/CdS) and 0.3 eV (CdSe/ZnCdS). In Eq.(1), $h\nu = 1.55$ eV (~ 800 nm) and a qualitative envelope W2PA is obtained using a (phenomenological) bandwidth of 40 meV, which corresponds to the convolution of the excitation laser bandwidth and the thermal broadening bandwidth for a single nanoparticle.

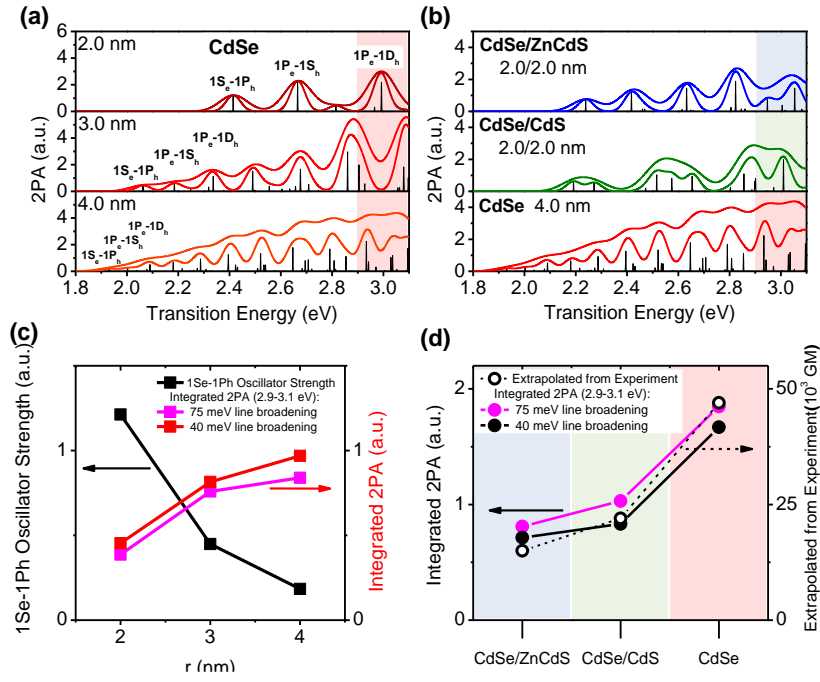


Figure S2. (a) Two-photon absorption spectra for different sizes of core-only CdSe QDs, the sharp peaks refer to the transitions and the curves refer to phenomenologically broaden transitions considering 40 meV and 75 meV bandwidth. (b) same as (a) but comparing different heterostructures with the same volume. (c) Comparison of the single transition oscillator strength and integrated oscillator strength for both bandwidth as a function of the CdSe QD radius. Note that changes in the simulation bandwidth do not alter the qualitative behavior. (d) Comparison of the integrated 2PA cross-section in the quasi-continuum region for all three types of structures with the same volume. The comparison considers the experimental data from Figure 2, and the theoretical model with different bandwidths. Note that the qualitative agreement between the experimental data and the model is independent of the bandwidth used in the model.

In fact, the phenomenological bandwidth used in our simulations do not influence the qualitative behavior of the integrated magnitude of σ_{2PA} in the quasi-continuum spectral

range. **Figure S2** shows how the integrated σ_{2PA} varies for different phenomenological bandwidths. For this comparison, we choose 40 meV, which is the homogeneous broadening at room temperature, and 75 meV, which is closer to the total broadening caused mostly by the inhomogeneous broadening of the samples. Note that, the qualitative behavior is the same for both situations.

Further insight into the secondary role of wave function overlaps is provided by analyzing CdSe/ZnCdS quantum dots (QDs) in more detail. In these structures, one may naively expect that transitions involving states localized in the core and states delocalized over the entire QD, because of the small overlap, yield smaller oscillator strength than in core only CdSe QDs. **Figure 4d** in the main text shows that this is not the case. To a large extent, this is explained by the behavior of intraband transitions. **Figure S3** shows the wave function of the first electron states in a CdSe/ZnCdS QD with dimensions 2.0/2.0 nm. As can be seen, the wave function delocalization into the shell is a gradual effect. Because the relevant intraband transitions involve $\Delta L = \pm 1$, which are consecutive states (recall **Figure 4a** in the main text), there is no drastic change in the wave function overlap as compared to core-only QDs. The same holds for CdSe/CdS QDs.

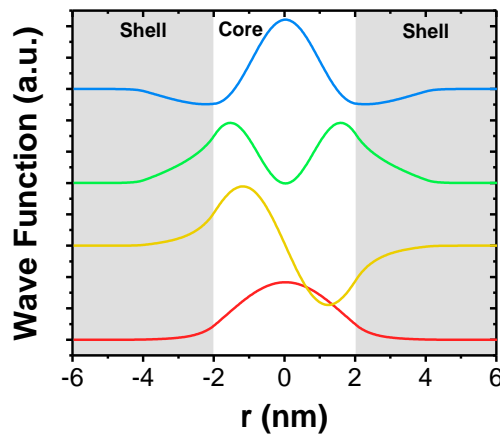


Figure S3. Lowest-lying electron wave functions in the CdSe/ZnCdS QD. The delocalization into the shell increases gradually.

Two-Photon Absorption Cross-Section Measurement Method

All two-photon absorption measurements were performed using a Ti:sapphire femtosecond amplified laser system and an optical parametric amplifier, all operating at 1 kHz and delivering pulses of about 100 fs (*FWHM*). The laser pulse width is measured by a home-built intensity autocorrelator by second harmonic generation. For all measurements, samples were suspended in toluene and kept in a 1-mm-thick spectroscopy-grade quartz cuvette.

Multiphoton Absorption by Photoluminescence Saturation - MPAPS

The two-photon absorption cross-section measurements were made with the Multiphoton Absorption by Photoluminescence Saturation (MPAPS) method.⁶ For two photon absorption (2PA, in a first approximation, this method assumes that semiconductor nanocrystals (NCs) have fast Auger recombination, which effectively suppresses multi-exciton emission. Consequently, NCs that absorb a pair or more of photons emit only one photon, and the integrated photoluminescence (PL) is given by

$$PL = \gamma(QY_X)(1 - P(0)) \quad (\text{S.1})$$

where γ is the collection/detection efficiency, QY_X is the emission quantum yield of the NC, and $P(0)$ is the probability that a NC does not absorb any photons. By modeling the probability of a NC having N excitons with Poisson statistics given the average number of excitons per NC is $\langle N \rangle$, we have $P(N) = \frac{\langle N \rangle^N e^{-\langle N \rangle}}{N!}$, and the PL becomes

$$PL = \gamma(QY_X)(1 - e^{-\langle N \rangle}) \quad (\text{S.2})$$

For quasi-type-II nanocrystals, Auger recombination can be slow, increasing the biexciton contribution to the PL. The fitting procedure accounts for contributions from

biexcitons.⁶ It is also possible to take into account the emission of biexciton species in the case of NCs with reduced Auger recombination rate by fitting the PL saturation using

$$PL = \gamma \left((1 - e^{-\langle N \rangle}) \left(1 + \frac{QY_{XX}}{QY_X} \right) - \frac{QY_{XX}}{QY_X} (\langle N \rangle e^{-\langle N \rangle}) \right) \quad (\text{S.3})$$

where QY_{XX} is the biexciton emission quantum yield.

The average number of excitons per NC can be calculated by

$$\langle N \rangle = \frac{\langle n \rangle}{2} = \frac{\sigma_2}{2\sqrt{2\pi}} \frac{\langle \Phi \rangle^2}{T} \quad (\text{S.4})$$

where $\langle n \rangle$ is the average number of absorbed photons, σ_2 is the 2PA cross-section, $\langle \Phi \rangle$ is the photon flux, and T is the excitation pulse-width ($HW \frac{1}{e} M$). The photon flux is defined

as $\langle \Phi \rangle = \frac{2E}{(\pi w^2)(\hbar\omega)}$, where E is the laser pulse energy, and w is the $HW/1/e^2$ beam spot size.

Finally, by replacing $\langle N \rangle$ from Eq. S.4 into Eq. S.3, one can use Eq. S.3 to fit the graph of PL vs $\langle \Phi \rangle^2$ as in **Figure S4**. Note that the only fitting parameters are σ_2 and γ , in which γ refers to the maximum amplitude of the measured signal.

More details for these expressions are available in Ref. ⁶.

The measured saturation curves for all samples discussed in the main text are shown in Figure S3. By observing the data, one can see the different size scaling for each type of structure.

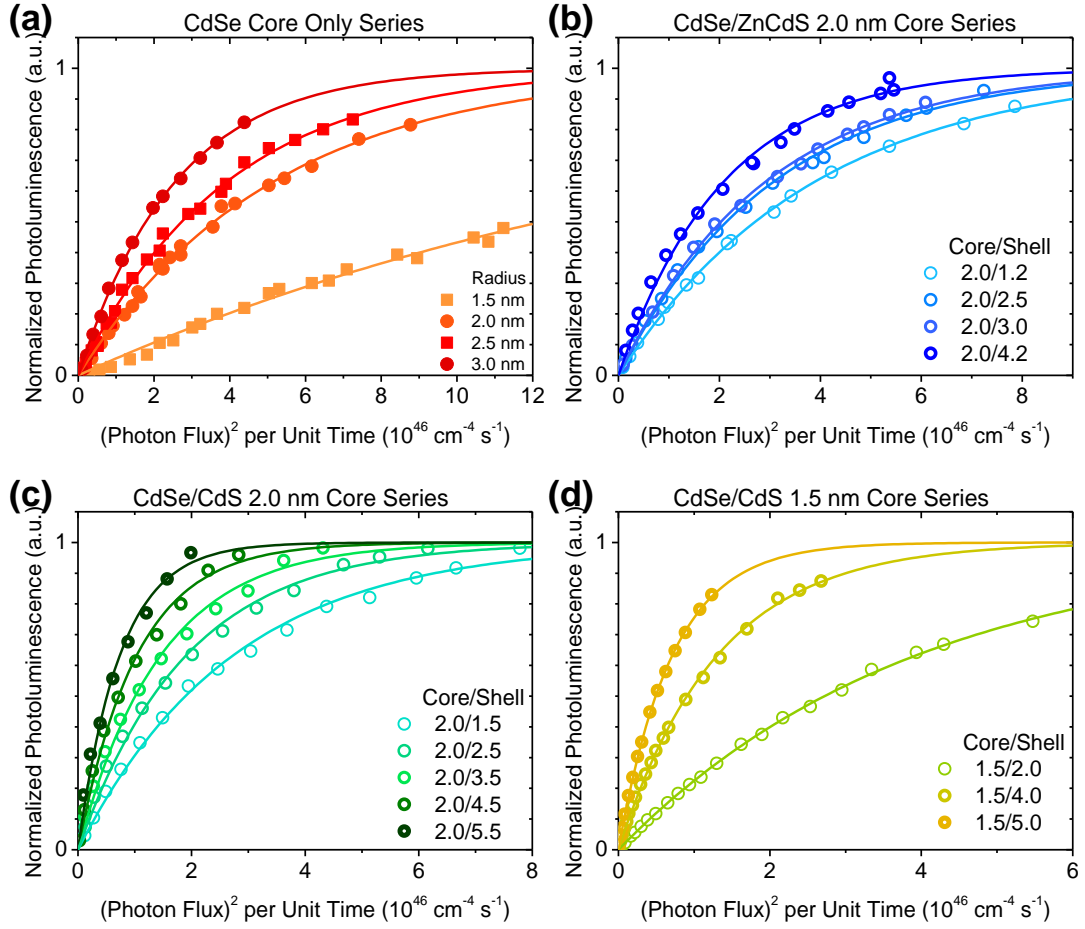


Figure S4. Experimental saturation curves at 800nm for (a) the CdSe core only, (b) the CdSe/ZnCdS type I core/shell, and the CdSe/CdS series with (c) 2.0 nm core radius and (d) 1.5 nm core radius.

For all samples, the fitting to the experimental data results with a value for σ_2 with a fitting error $\frac{\Delta\sigma_{2,fit}}{\sigma_{2,fit}} \lesssim 10\%$. Note that, because for a given series of samples, all samples were measured under the same experimental conditions, this is the relative error for their values of σ_2 . However, the absolute error needs to consider the experimental error due to the uncertainties on the laser beam characterization. As it is described in details in Ref. 6, the experimental error due to the laser characterization is on the order of $\frac{\Delta\sigma_{2,laser}}{\sigma_{2,laser}} 15\%$. Consequently, one can estimate the absolute error by

$$\frac{\Delta\sigma_2}{\sigma_2} = \sqrt{\left(\frac{\Delta\sigma_{2,fit}}{\sigma_{2,fit}}\right)^2 + \left(\frac{\Delta\sigma_{2,laser}}{\sigma_{2,laser}}\right)^2} \cong 20\% \quad (\text{S.5})$$

And this is the error bar consider throughout the manuscript (see Figs. 2, 3, and 5).

Additionally, for our samples, the ratio between biexciton, QY_{XX} , and single exciton, QY_X , emission quantum yield is $\frac{QY_{XX}}{QY_X} \lesssim 0.1$, agreeing with previously reported value.⁷ From time resolved PL measurements, QY_{XX} is estimated from the ratio between biexciton and single-exciton PL lifetimes, according to

$$\frac{QY_{XX}}{QY_X} = 4 \frac{\tau_{XX}}{\tau_X} \quad (\text{S.6})$$

For abrupt interface CdSe/CdS heterostructures, $\frac{QY_{XX}}{QY_X} < 10$,⁷ consequently, the correction for the influence of the multi-exciton emission is minimal. **Figure S5** illustrates the multi-exciton contribution for the two CdSe/CdS heterostructures with thicker shell, which are the ones more likely to have biexciton emission. Note that the largest value for $\frac{QY_{XX}}{QY_X}$ is 0.075. Even though the correction is small, they are considered in the fittings according to Eq. S.3 for samples with thick shell.

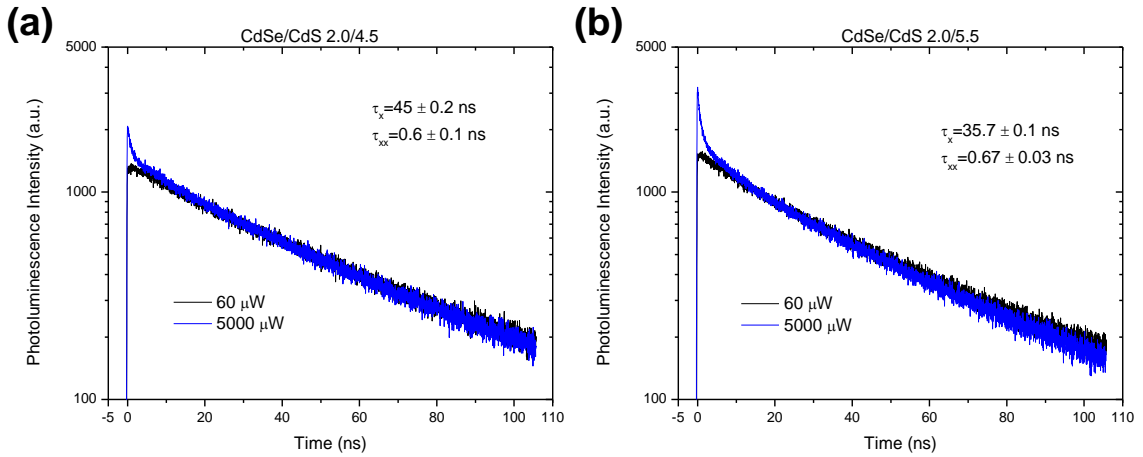


Figure S5. Time correlated single photon counting data for the CdSe/CdS 2.0 nm core samples with (a) 4.5 nm shell and (b) 5.5 nm shell.

Table S1: Quantum yield data for the CdSe and CdS samples.

Sample		Quantum Yield (%)
CdSe	1.5	6 ± 1
	2.0	15 ± 1
	2.5	9 ± 1
	3.0	9 ± 1
CdSe/CdS	2.0/1.5	84 ± 2
	2.0/2.5	91 ± 6
	2.0/3.5	90 ± 10
	2.0/4.5	78 ± 6
	2.0/5.5	55 ± 2
	1.5/2.0	88 ⁸
	1.5/4.0	70 ⁸
	1.5/5.0	66 ⁸

Two-Photon-Excited Photoluminescence – 2PEP

The 2PA spectra shown in Figure 2 were measured by 2PEP following the method described in details by Xu and Webb⁹ and Makarov et.al.¹⁰ When appropriated, Rhodamine B in Methanol has been used as reference sample for the measurement in order to obtain the magnitude for σ_2 following the equation

$$\sigma_{2,s} = \frac{c_{ref} QY_{ref} n_{ref} \langle PL \rangle_s E_{ref}^2}{c_s QY_s n_s \langle PL \rangle_{ref} E_s^2} \sigma_{2,ref} \quad (S.7)$$

In which, c refers to the concentration, QY to the single exciton emission quantum yield, n the solvent refractive index, $\langle PL \rangle$ the temporally and spectrally integrated PL, and E to the exciting pulse energy. The sub-index “s” and “ref” refer to the parameters for the sample and reference, respectively.

For each excitation wavelength, $\langle PL \rangle$ is collected for at least 3 different pump pulse energies to verify its quadratic dependence, to make sure the experiment is performed far from the saturation limit.

As one can see in Eq. S.7, in this experiment, the magnitude of $\sigma_{2,s}$, depends on up to 10 other parameters from the sample and from the reference, which introduces large relative and absolute errors to the measured values. To minimize that, we use the $\sigma_{2,s}$ values obtained by MPAPS to rescale the 2PEP data in Figure 2 of the main text.

Samples Synthesis Methods

Materials. Cadmium oxide (CdO, 99.95%) and selenium powder (Se, 100 mesh, 99.99%) were purchased from Alfa Aesar. 1-dodecanethiol (DDT, 98%) was purchased from Sigma Aldrich. Zinc acetate (Zn(ac)₂, 99.9 %), sulfur powder (S₈, 99.9 %), oleic acid (OA, 99 %), 1-octadecene (ODE, 99 %), tri-n-octylamine (TOA, 99%), and tri-n-octylphosphine (TOP, 99 %) were purchased from Uniam.

Precursor preparation. All chemistry is carried out under the Schlenk line technique. 0.5 M cadmium oleate (Cd(OA)₂), 0.5 M zinc oleate (Zn(OA)₂), 1 M tri-n-octylphosphine selenium (TOPSe), 1 M tri-n-octylphosphine sulfur (TOPS) and 0.5 M DDT (diluted with TOA) stock solution are prepared before the CdSe, CdSe/CdS and CdSe/ZnCdS QD synthesis. For Cd(OA)₂ preparation, 50 mmol of CdO and 100 mmol of OA are mixed in a three-neck flask (250 ml), degassed at 130 °C for 1 hour, backfilled with N₂, and heated up to 300 °C to form optically clear Cd(OA)₂ solution. The solution is diluted with TOA to a total volume of 100 ml. Zn(OA)₂ is prepared following the above procedure (Cd(OA)₂) with Zn(ac)₂ in replace of CdO. 1 M TOPSe was prepared by stirring 20 mmol

of Se with 20 mL of TOP at 160 °C for 5 hours. 1M TOPS was prepared in the same procedure with S in replace of Se at 60 °C.

CdSe core synthesis. CdSe cores are synthesized following the previously reported method¹¹ with minor modifications. 1 ml of 0.5 M Cd(OA)₂, 0.25 mmol of Se powder, and 5 ml of ODE are degassed at room temperature (RT) for 5 minutes in a 3-neck round flask and backfilled with N₂. The solution is heated to 240 °C and maintained for 5 min (30 min), resulting in CdSe QDs with a radius of 1.5 nm (2 nm). Additional injection of 0.6 ml of 0.5 M Cd(OA)₂ and 0.15 ml of 1 M TOPSe leads to further growth of CdSe cores to a radius of 3 nm. CdSe cores are purified twice by precipitation (ethanol)/redispersion (toluene) method and finally redispersed in 5 ml of toluene.

Type-I CdSe/ZnCdS (CdSe/Zn_{0.5}Cd_{0.5}S) QD synthesis. Type-I CdSe/ZnCdS QDs are synthesized following the previously reported method¹² with minor modifications. A reaction flask containing 10 ml of TOA and 300 mg of CdSe cores ($r = 2$ nm) is degassed at 130 °C for 30 minutes, backfilled with N₂ and heated up to 300 °C. 1.5 ml of 0.5 M Cd(OA)₂, 3 ml of 0.5 M Zn(OA)₂ and 2 ml of 1 M TOPS are injected dropwise to the reaction flask for 1.2 nm of Cd_{0.5}Zn_{0.5}S shell growth. The injecting volume of Cd(OA)₂, Zn(OA)₂, and TOPS are varied for the Cd_{0.5}Zn_{0.5}S shell thickness control. The resulting CdSe/ZnCdS QDs are purified repeatedly for further characterization.

Quasi-Type-II CdSe/CdS QD synthesis. Quasi-Type-II CdSe/CdS QDs are synthesized following the previously reported method⁷ with minor modifications. A reaction flask containing 10 ml of TOA and 300 mg of CdSe cores ($r = 2$ nm) is degassed at 130 °C for 30 minutes, backfilled with N₂, and heated up to 300 °C for further CdS shell growth. 15 ml of 0.5 M Cd(OA)₂ and 0.5 M DDT are injected at a rate of 2 ml/h into the reaction flask for 5.5 nm of CdS shell. The reaction was maintained at 300 °C during CdS shell

growth. The injecting volume of Cd(OA)₂ and DDT are controlled for CdS shell growth on the varying radius of CdSe cores ($r = 1.5, 2.5, 3.0$ nm). The resulting QDs are purified fifth in the same way as CdSe core synthesis for further characterization.

Samples morphological details. All CdSe-based QDs used in this study are zinc blende. We have measured the size (and distribution) of CdSe core QDs from TEM analysis and, validated them with the estimations from $1S_e-1S_h$ transition wavelength seen in UV-Vis spectra at room temperature. We adopt the fast shell growth methods to prepare the core/shell QD samples with an abrupt interface, consequently, no significant interfacial alloying is expected in these core/shell samples as described in Ref. ⁷

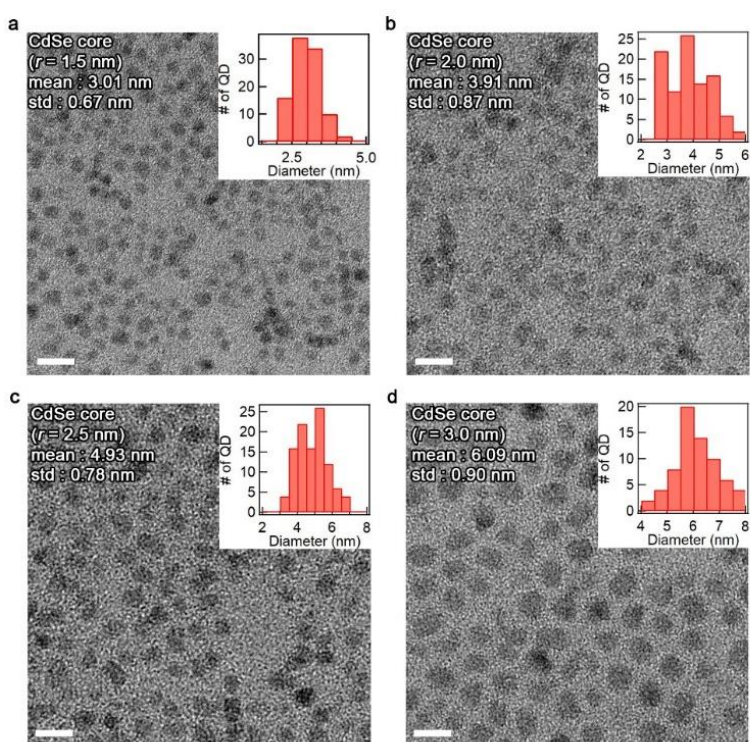


Figure S6. TEM images of CdSe cores with varying radii ($r =$ (a) 1.5 nm, (b) 2.0 nm, (c) 2.5 nm, and (d) 3.0 nm). The insets show the size distributions of each CdSe core. Scale bars = 10 nm.

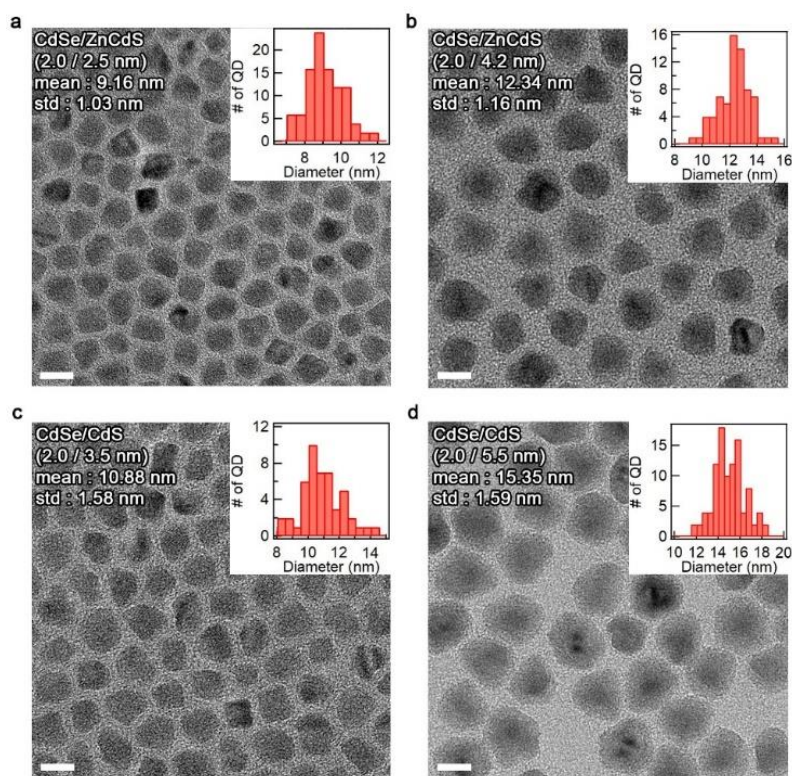


Figure S7. TEM images of (a,b) CdSe ($r = 2.0$ nm)/ZnCdS QDs and (c,d) CdSe ($r = 2.0$ nm)/CdS QDs with different shell thicknesses. The insets show size distribution of each sample. Scale bars = 10 nm.

References

- (1) Allione, M.; Ballester, A.; Li, H.; Comin, A.; Movilla, J. L.; Climente, J. I.; Manna, L.; Moreels, I. Two-photon-induced blue shift of core and shell optical transitions in colloidal CdSe/CdS quasi-type II quantum rods. *ACS Nano* **2013**, *7*, 2443-2452.
- (2) Aubert, T.; Golovatenko, A. A.; Samoli, M.; Lermusiaux, L.; Zinn, T.; Abécassis, B.; Rodina, A. V.; Hens, Z. General expression for the size-dependent optical properties of quantum dots. *Nano Lett.* **2022**, *22*, 1778-1785.
- (3) Adachi, S. *Handbook on physical properties of semiconductors*; Springer Science & Business Media, 2004.
- (4) Rainò, G.; Stöferle, T.; Moreels, I.; Gomes, R.; Kamal, J. S.; Hens, Z.; Mahrt, R. F. Probing the wave function delocalization in CdSe/CdS dot-in-rod nanocrystals by time- and temperature-resolved spectroscopy. *ACS Nano* **2011**, *5*, 4031-4036.
- (5) Xie, R.; Kolb, U.; Li, J.; Basché, T.; Mews, A. Synthesis and characterization of highly luminescent CdSe–Core CdS/Zn_{0.5}Cd_{0.5}S/ZnS multishell nanocrystals. *J. Am. Chem. Soc.* **2005**, *127*, 7480-7488.
- (6) Alo, A.; Barros, L. W.; Nagamine, G.; Vieira, L. B.; Chang, J. H.; Jeong, B. G.; Bae, W. K.; Padilha, L. A. Simple yet effective method to determine multiphoton absorption cross section of colloidal semiconductor nanocrystals. *ACS Photon.* **2020**, *7*, 1806-1812.
- (7) Bae, W. K.; Padilha, L. A.; Park, Y.-S.; McDaniel, H.; Robel, I.; Pietryga, J. M.; Klimov, V. I. Controlled alloying of the core–shell interface in CdSe/CdS quantum dots for suppression of Auger recombination. *ACS Nano* **2013**, *7*, 3411-3419.

- (8) Jeong, B. G.; Park, Y.-S.; Chang, J. H.; Cho, I.; Kim, J. K.; Kim, H.; Char, K.; Cho, J.; Klimov, V. I.; Park, P. Colloidal spherical quantum wells with near-unity photoluminescence quantum yield and suppressed blinking. *ACS Nano* **2016**, *10*, 9297-9305.
- (9) Xu, C.; Webb, W. W. Measurement of two-photon excitation cross sections of molecular fluorophores with data from 690 to 1050 nm. *J. Opt. Soc. Am. B-Opt. Phys.* **1996**, *13*, 481-491.
- (10) Makarov, N. S.; Drobizhev, M.; Rebane, A. Two-photon absorption standards in the 550–1600 nm excitation wavelength range. *Opt Express* **2008**, *16*, 4029-4047.
- (11) Yang, Y. A.; Wu, H.; Williams, K. R.; Cao, Y. C. Synthesis of CdSe and CdTe nanocrystals without precursor injection. *Angew. Chem.* **2005**, *117*, 6870-6873.
- (12) Lim, J.; Jeong, B. G.; Park, M.; Kim, J. K.; Pietryga, J. M.; Park, Y. S.; Klimov, V. I.; Lee, C.; Lee, D. C.; Bae, W. K. Influence of Shell Thickness on the Performance of Light-Emitting Devices Based on CdSe/Zn_{1-x}Cd_xS Core/Shell Heterostructured Quantum Dots. *Adv. Mater.* **2014**, *26*, 8034-8040.